Copyright © 2002 IFAC
15th Triennial World Congress, Barcelona, Spain

ESTIMATION OF AUTOMOTIVE TIRE FORCE CHARACTERISTICS USING WHEEL VELOCITY

Eiichi Ono*, Katsuhiro Asano*, Masaru Sugai*, Shoji Ito, Akira Tanaka**, Mamoru Sawada*** and Yoshiyuki Yasui******

** Toyota Central R & D Labs. Inc., ** Toyota Motor Corporation, *** Denso Corporation, **** Aisin Seiki Co., Ltd.*

Abstract: It is important to estimate friction force characteristics between tire and road in order to improve the control performance of a vehicle in critical motions. In this paper, an estimation method which estimates parameters concerned with friction force margin is proposed by applying the on-line least squares method to wheel rotational velocities. The effect of the estimation is evaluated by applying the method to the braking control. *Copyright © 2002 IFAC*

Keywords: automobiles, vehicle dynamics, wheels, velocity, least-squares estimation, brakes, tyres, friction, servo, control.

1. INTRODUCTION

For analysis and computer simulation, various tire models for automotive vehicles are proposed (Bernard *et al*., 1977; Bakker *et al*., 1987). If the friction force margin of each wheel can be estimated by using tire models, it is expected that the control performance of the vehicle can be improved. However, the parameters of the tire model are changed depending on condition of tire and road. Then, it is difficult to use the tire model for estimating friction force margin, and a robust control approach which treats tire characteristics as plant perturbations is proposed (Ono and Hosoe, 2000).

In this paper, we estimate friction force characteristics between tire and road using wheel velocity. The parameter concerned with friction force margin is estimated by the method. The method brings high performance vehicle control which cannot be achieved by the robust control approach.

The slope of friction force against slip velocity at the operational point, or Extended Braking Stiffness (hereafter "XBS"), is an important parameter of tire/road friction characteristics. Maximum braking force can be obtained at the point XBS=0 (see Fig. 1), and a decrease in XBS indicates a decrease in the margin of friction force.

In the following sections, we propose the estimation method of XBS from wheel velocity by applying the on-line least squares method.

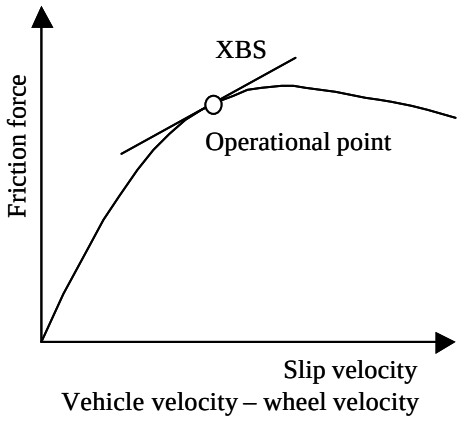

Fig. 1. Tire/road characteristics and extended braking stiffness (XBS)

Further, we evaluate the proposed method by applying XBS to the braking control.

2. ESTIMATION OF EXTENDED BRAKING STIFFNESS (XBS)

2.1 Wheel deceleration model

The pneumatic tires of the vehicle have rotational resonance from the wheel inertia and the sidewall spring (Umeno *et al*., 2002). However, the resonance vanishes when braking because of brake pad friction. Then, the rotational dynamics of the wheel (see Fig. 2) are modeled by the equation

$$J\dot{v}_w = r^2 F_x - rT + r^2 d, \qquad (1)$$

where,

- J : moment of inertia of wheel,
- r : radius of wheel,
- F_x : friction reaction force between tire and road,
- T : brake torque (in proportion to wheel cylinder pressure),
- d : disturbance from road, and
- v_w : wheel velocity.

By assuming that vehicle dynamics are sufficiently slower than wheel dynamics and F_x is a function of slip velocity, the Wheel Deceleration Model can be obtained from (1).

$$\ddot{v}_w = -\frac{kr^2}{J}\dot{v}_w + w \qquad (2)$$

Here,

- k : Extended Braking Stiffness (XBS),
- w : disturbance from road and brake torque fluctuations ($w = r^2\dot{d} - r\dot{T}$).

If we assume constant deceleration braking, for example, m-peak braking on constant m road, brake torque T can be treated as a disturbance by differentiating (1). This implies that XBS can be estimated from wheel velocity. It is not necessary to use the wheel cylinder pressure value. (2) describes the dynamics of wheel deceleration, and XBS is proportionate to the break point frequency of the wheel deceleration model. Then, XBS can be estimated by identifying the break point frequency of (2).

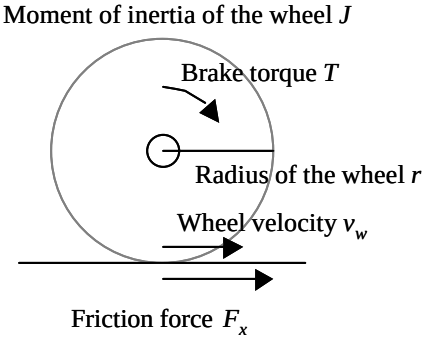

Fig. 2. Rotational dynamics of the wheel

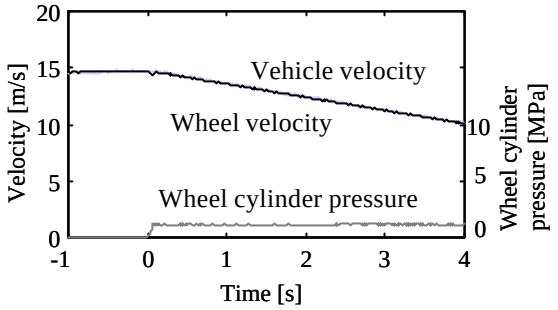

(a) Soft braking: Wheel cylinder pressure = 1MPa

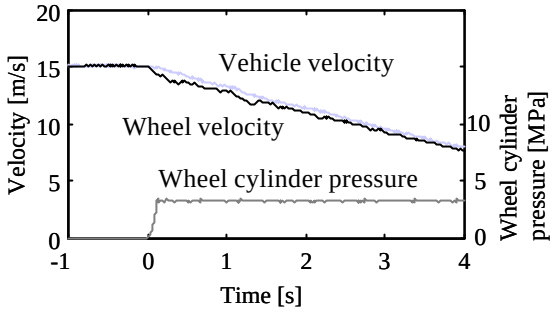

(b) Hard braking: Wheel cylinder pressure = 3MPa

Fig. 3. Experimental results of the vehicle braking with constant wheel cylinder pressure on packed snow road.

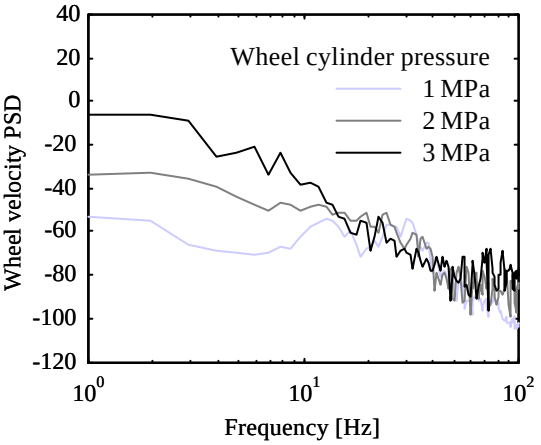

Fig. 4. Experimental results of the frequency characteristics of wheel velocity with constant wheel cylinder pressure on packed snow road. Hard braking: wheel cylinder pressure = 3 MPa (Fig. 3 (b)), moderate braking: wheel cylinder pressure = 2 MPa, soft braking: wheel cylinder pressure = 1 MPa (Fig. 3 (a)).

Figure 3 shows experimental results of the vehicle braking with constant wheel cylinder pressure on packed snow road. While there is sufficient margin of friction force in Fig. 3 (a), it shows critical braking near m-peak in Fig. 3 (b).

Figure 4 shows the experimental results of the frequency characteristics of wheel velocity shown in

Fig. 3 during braking. The magnitude of power spectrum density in low frequency increases according to the increase in wheel cylinder pressure, and break point frequency shifts to the left (low frequency). This indicates that XBS decreases according to the decrease in margin of friction force.

2.2 Applying on-line least squares method

By assuming that w is white noise, XBS k can be estimated by applying the least squares method (Ljung, 1987) to (2) as follows:

$$\phi[i] = \frac{\tau r^2}{J}(v[i-1] - v[i-2]) \quad (3)$$

$$y[i] = -v[i] + 2v[i-1] - v[i-2] \quad (4)$$

$$L[i] = -\frac{P[i-1]\phi[i]}{\lambda + \phi[i]^2 P[i-1]} \quad (5)$$

$$P[i] = -\frac{1}{\lambda}\left[P[i-1] - \frac{\phi[i]^2 P[i-1]^2}{\lambda + \phi[i]^2 P[i-1]}\right] \quad (6)$$

$$\hat{k}[i] = \hat{k}[i-1] + L[i]\left(y[i] - \phi[i]\hat{k}[i-1]\right) \quad (7)$$

Here,

τ : sampling time,
v : filtered (2-20 Hz band pass) wheel velocity,
$\hat{k}$: estimated XBS, and
λ : forgetting factor.

The algorithm described by (3)-(7) estimates XBS from the fluctuation phenomenon of wheel velocity. Figure 5 shows estimated XBS by (3)-(7) of the experimental result shown in Fig. 3 (b). XBS is on the decrease according to hard braking.

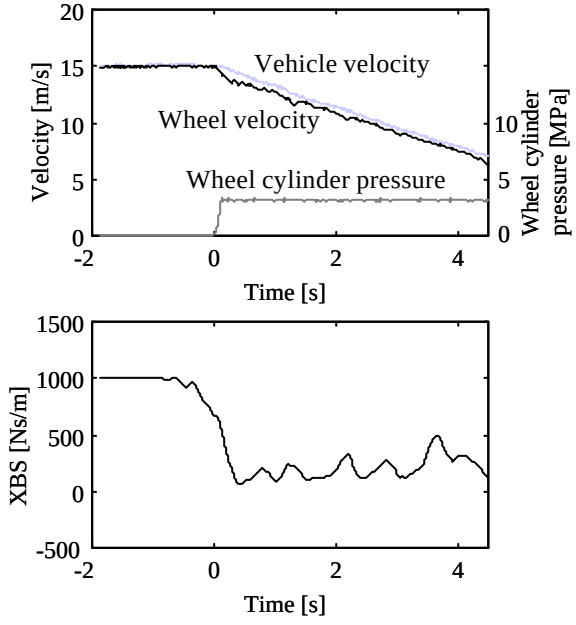

Fig. 5. Estimated XBS by (3)-(7) of the experimental results shown in Fig. 3 (b)

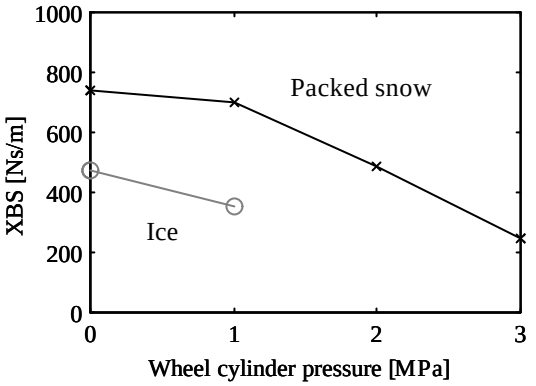

Fig. 6. Relation between averaged XBS during braking and wheel cylinder pressure

Figure 6 shows the relation between averaged XBS during braking and wheel cylinder pressure. According to the decrease in margin of friction force on each road surface, estimated XBS is on the decrease. This implies that the maximum braking force on each road surface can be obtained by the XBS servo control, i. e., actuation of wheel cylinder pressure which controls estimated XBS to the small value.

3. EVALUATION OF ESTIMATED XBS

The estimated XBS can be applied for brake controls, e.g. ABS. In this paper, we propose the brake control which obtains a constant μ rate to evaluate the XBS estimation method. For an experimental vehicle, a conventional ABS actuator is used. However, the conventional on-off ABS valves may not be suitable for the proposed system. Therefore, we only evaluate ABS performance such as stopping distance, steerability and stability. Noise and vibration due to the conventional ABS valves are not evaluated.

3.1 XBS servo control

A control system to follow the reference value of XBS (XBS servo control) is realized by a 3 layered hierarchy control as shown in Fig. 7. In order to follow the reference of XBS, the XBS servo calculates the reference value of wheel deceleration, the deceleration servo calculates the reference value of the pressure of the wheel cylinder, and the brake servo calculates the valve command of ABS.

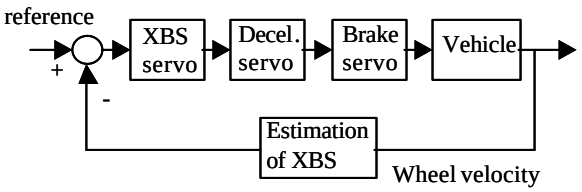

Fig. 7. Control system structure of XBS servo

Since estimation of XBS uses the fluctuation phenomenon of wheel velocity, the deceleration servo influences the estimation of XBS. The deceleration servo works on the stabilization of wheel dynamics.

The Wheel Deceleration Model with the deceleration servo can be described as

$$\ddot{v}_e = -\left(a + \frac{kr^2}{J} \right) \dot{v}_e + w. \quad (8)$$

Here,

$$\dot{v}_e = \dot{v}_w - \dot{v}_0, \quad (9)$$

$\dot{v}_0$: reference value of deceleration servo, and

a : feedback gain of deceleration servo.

Then, the estimation algorithm is modified as

$$\hat{k}_d[i] = \hat{k}[i] - \frac{J}{r^2} a. \quad (10)$$

Here,

$\hat{k}_d$: estimated value of XBS under the deceleration servo.

From (8), it is obvious that the robust stability of the deceleration servo is compensated by designing feedback gain as

$$a > -\frac{k_{\min} r^2}{J}, \quad (11)$$

where,

$k_{\min}$: minimum value of XBS at arbitrary slip velocity on various roads.

3.2 Braking control strategy based on XBS

Friction force characteristics during combined steering and braking maneuvers are described by the brush model (Bernard *et al*., 1977). In this paper, the following variables are defined in order to simplify the model.

$$\kappa_x = \frac{s}{1-s} = \frac{v_x - v_w}{v_w} \quad (12)$$

$$\kappa_y = \frac{K_b v_y}{K_s v_w} \quad (13)$$

$$\kappa = \sqrt{\kappa_x^2 + \kappa_y^2} \quad (14)$$

Here,

s : slip rate,

v_x : longitudinal velocity of wheel,

v_y : lateral velocity of wheel,

K_s : longitudinal stiffness of tire, and

K_b : lateral stiffness of tire.

Assuming that the direction of the friction force θ coincides with the slip direction, as

$$\tan\theta = \frac{\kappa_x}{\kappa_y}, \quad (15)$$

the friction force can be described as follows.

Case 1: $\sigma_s = 1 - \frac{K_s}{3\mu F_z}\kappa > 0$

$$F_x = \mu F_z \cos\theta \left(1 - \sigma_s^3\right) \quad (16)$$

$$F_y = \mu F_z \sin\theta \left(1 - \sigma_s^3\right) \quad (17)$$

Case 2: $\sigma_s = 1 - \frac{K_s}{3\mu F_z}\kappa < 0$

$$F_x = \mu F_z \cos\theta \quad (18)$$

$$F_y = \mu F_z \sin\theta \quad (19)$$

Here,

μ : maximum friction coefficient,

F_x : longitudinal friction force,

F_y : lateral friction force, and

F_z : load force.

Further, we define μrate (i.e. generated friction force / maximum friction force) as

$$\eta = \frac{F}{\mu F_z} = \frac{\sqrt{F_x^2 + F_y^2}}{\mu F_z}. \quad (20)$$

From (12)-(20), the slope of friction force F against slip κ can be described using $\eta\ (0 \le \eta < 1)$ as

$$\frac{\partial F}{\partial \kappa} = K_s (1-\eta)^{\frac{2}{3}} \quad (21)$$

$\partial F / \partial \kappa$ is described as a function of K_s and η. This means that a constant μrate is obtained by a control which gives a constant $\partial F / \partial \kappa$, even if the maximum friction coefficient μ changes. Furthermore, XBS k can be described as

$$k = \frac{\partial F_x}{\partial \kappa_x} \cdot \frac{1}{v_w} = \frac{K_s}{v_w} \left[(1-\eta)^{\frac{2}{3}} \cos^2\theta + \frac{\sin^2\theta}{3} \left\{ 1 + (1-\eta)^{\frac{1}{3}} + (1-\eta)^{\frac{2}{3}} \right\} \right]. \quad (22)$$

This means that a constant μrate is obtained by the XBS servo control that follows (22). In (22), force direction θ can be estimated from steer angle and vehicle velocity.

4. EXPERIMENTAL RESULTS

4.1 Braking on constant μ road

Figure 8 and Figure 9 show experimental results of straight line braking on an artificial low friction road with the XBS servo which follows (22) and conventional ABS. Fluctuations of wheel velocity and the pressure of the wheel cylinder are suppressed by the XBS servo and a larger friction force is obtained than with conventional ABS.

Figure 10 shows F_x - κ_x plot, the approximated brush model and the operational point of the XBS servo on an artificial low friction road. In order to measure F_x - κ_x plot, the wheel cylinder pressure of front wheels equipped with wheel dynamometers (Burkard and Calame, 1998) increases at a constant rate until the front wheels are locked (Yasui *et al*., 2000). Vehicle velocity is also measured by optical sensor, and κ_x is calculated by (12). The parameters K_s and μ of the brush model (16) are decided so that the model

approximates to F_x - κ_x plot. The operational point of the XBS servo indicates average F_x and κ_x during XBS servo operation (experimental result shown in Fig. 8). Each experiment, i. e. measurement of friction force characteristics and the XBS servo, has the same initial velocity of 15 m/s. Figure 10 also shows average value of $\partial F_x/\partial \kappa_x$ calculated by multiplying the estimated XBS by v_w. This figure shows that desirable friction force can be obtained by the XBS servo.

The effect of the XBS servo during combined steering and braking maneuvers is shown in Fig. 11. The brake is applied on vehicles turning with a constant steering wheel angle on an artificial low friction road from an initial velocity of 15 m/s, and the longitudinal and lateral forces of the front wheels are measured by wheel dynamometers. Figure 11 shows the average longitudinal friction coefficient $(\mu_x = F_x/F_z)$ and the lateral friction coefficient $(\mu_y = F_y/F_z)$ for 2 seconds from applying the brake.

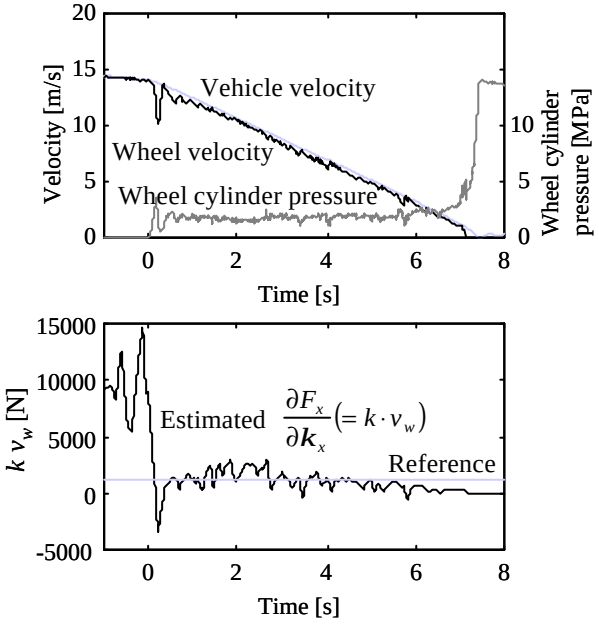

Fig. 8. Experimental results with XBS servo on artificial low friction road

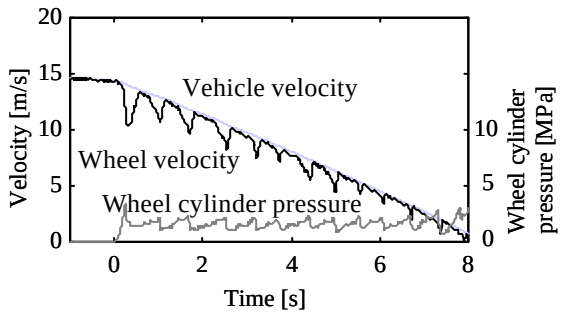

Fig. 9. Experimental results with conventional ABS on artificial low friction road

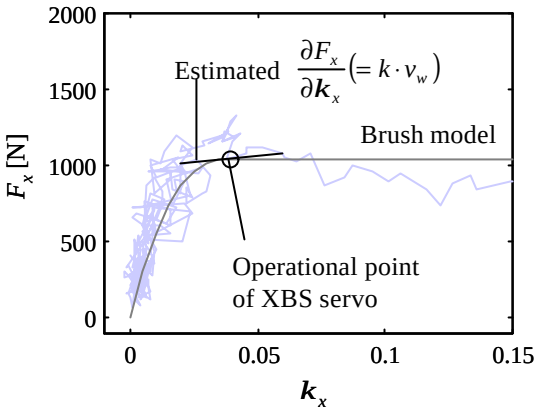

Fig. 10. Friction force characteristics on artificial low friction road

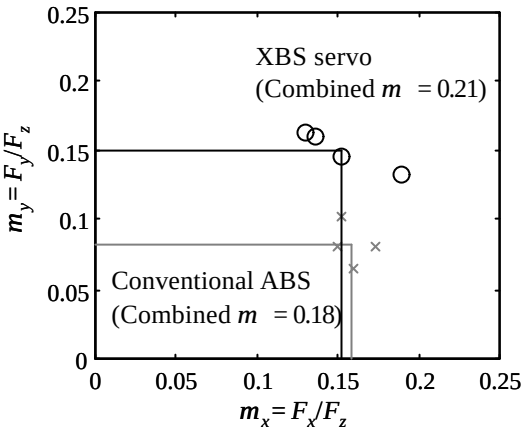

Fig. 11. Friction force characteristics on artificial low friction road

The points O and X indicate four experimental results of the XBS servo and conventional ABS, respectively. This figure shows that combined μ $\left(=\sqrt{\mu_x^2+\mu_y^2}\right)$ is also improved by the XBS servo.

4.2 Adaptation to change of road friction characteristics

XBS servo avails a μpeak following control even if maximum friction coefficient μ changes. In this section, we evaluate the adaptation of the XBS servo to changes in road friction characteristics. Figure 12 shows the experimental results of the XBS servo during changes in road friction characteristics from an artificial low friction road to a dry road.

When the vehicle transitions from an artificial low friction road to a dry road, estimated $\partial F_x/\partial \kappa_x$ increases according to the increase in the margin of friction force. Then, the XBS servo works to increase wheel cylinder pressure more rapidly than conventional ABS, as shown in Fig. 13.

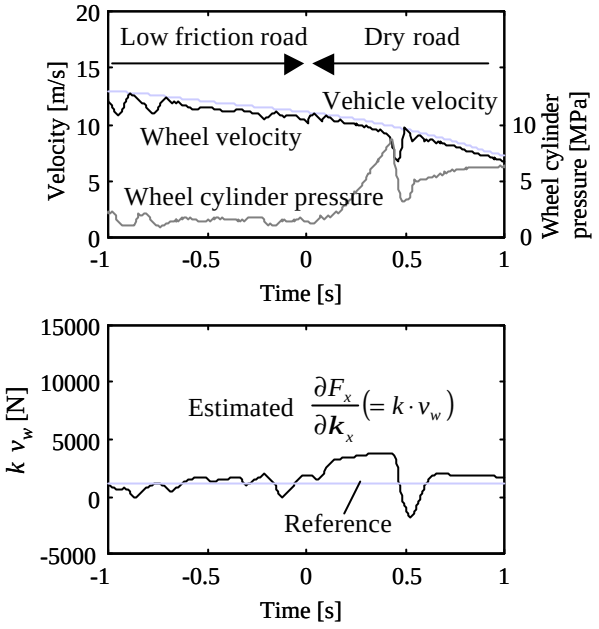

Fig. 12. Experimental results of XBS servo during change of road friction characteristics from artificial low friction road to dry road

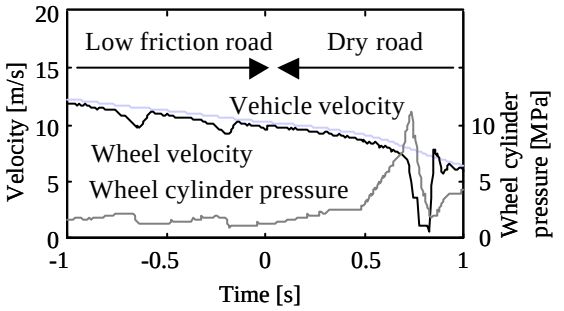

Fig. 13. Experimental results of conventional ABS during changes in road friction characteristics from artificial low friction road to dry road

5. CONCLUSION

XBS is an important parameter in identifying tire/road friction characteristics. In this paper, the estimation method of XBS is proposed and the performance of the XBS estimation is experimentally verified. Furthermore, we demonstrate the XBS servo control which obtains a constant m rate as compared with conventional ABS. In the future, we expect that XBS can be applied for brake control systems, e.g. Electro Hydraulic Brake EHB (Jonner *et al*., 1996; Leffler, 1996) and Electro Mechanical Brake EMB (Maron *et al*., 1997), to greatly enhance vehicle control performance.

REFERENCES

Bakker, E., L. Nyborg and H. B. Pacejka (1987). Tyre modelling for use in vehicle dynamics studies, *SAE paper*, 870421.

Bernard, J. E., L. Segel and R. E. Wild (1977). Tire shear force generation during combined steering and braking maneuvers. *SAE paper*, 770852.

Burkard, H. and C. Calame (1998). Rotating wheel dynamometer with high frequency response. *Tire Technology International 1998*, pp. 154-158.

Jonner, W. D., H. Winner, L. Dreilich and E. Schunck (1996). Electrohydraulic brake system, The first approach to brake-by-wire technology. *SAE paper*, 960991.

Leffler, H. (1996). Electronic brake management EBM, Prospects of an integration of brake system and driving stability control. *SAE paper*, 960954.

Ljung, L (1987). *System Identification, Theory for the user*. pp. 305-311, Prentice-Hall.

Maron, C., T. Dieckmann, S. Hauck and H. Prinzler (1997). Electromechanical brake system, Actuator control development system. *SAE paper*, 970814.

Ono, E. and S. Hosoe (2000). Techniques in vehicle integrated control for steering and traction systems. In: *Mechatronic systems techniques and applications: Volume 2 Transportation and vehicular systems* (Leondes, C. T. (Ed)), pp. 99-149. Gordon and Breach Science Publishers.

Umeno, T., E. Ono, K. Asano, A. Tanaka, S. Ito, Y. Yasui and M. Sawada (2002). Estimation of tire-road friction using tire vibration model, To appear in *SAE paper*.

Yasui, Y., H. Nitta, T. Yoshida, T. Hosome and K. Kawamura (2000). Experimental approach for evaluating tire characteristics and ABS performance. *SAE paper*, 2000-01-0110.